DOI: 10.1002/ejic.201100019

Synthesis and Reactivity of a New Oxidation-Labile Heterobimetallic Mn_6Zn_2 Carbamate Cluster and Precursor to Nanosized Magnetic Oxide Particles

Dan Domide,[a] Olaf Hübner,[a] Silke Behrens,[a] Olaf Walter,[b] Hubert Wadepohl,[a] Elisabeth Kaifer,[a] and Hans-Jörg Himmel*[a]

Keywords: Zinc / Manganese / Cluster compounds / Magnetic properties / Oxido ligands / Oligonuclear complexes / Carbamates

The synthesis and characterization of the new octanuclear mixed carbamate complex $[Zn_2Mn_6(\mu_4\text{-}O)_2(O_2CN(i\text{Pr})_2)_{12}]$ is reported. This complex is readily oxidized by O_2 to give $[Zn_2Mn_6(\mu_4\text{-}O)_2(\mu_3\text{-}O)(O_2CN(i\text{Pr})_2)_{12}]$ featuring a central O atom statistically distributed over two sites within the void of the inner Mn_6 cage of the carbamate complex. In relation to the situation before oxidation, the metal cage is expanded by a change of the carbamate bonding mode. The two carbamate complexes were used as precursors to magnetic oxide nanoparticles under mild conditions (210–270 °C depending on the heating rate). A mixture of crystalline $ZnMn_2O_4$ and MnO nanoparticles resulted. The experimental data are complemented by some quantum chemical (DF) calculations.

Introduction

Carbamates are of interest for a number of reasons. Hence they can be used as precursors for oxide thin films or nanoparticles.[1,2] In addition carbamate complexes of the elements zinc and magnesium were identified at the active site of phosphotriesterase and rubisco enzymes. The active site of rubisco consists of an octahedrally coordinated Mg atom, one of the ligands being a presumably κ^1-coordinated carbamate.[3] In Zn-containing phosphotriesterase two Zn atoms are bridged by a carbamate ligand.[4] A number of carbamate complexes of main group, transition metal and lanthanide elements have been synthesized in the past. Of the many examples, we briefly present some complexes with four or more metals. The tetranuclear Zn carbamate complexes $Zn_4(\mu_4\text{-}O)(O_2CNR_2)_6$ (e.g., R = Et)[5–6] could be regarded as a molecular model for ZnO.[7] They were indeed used as single-source precursors for chemical vapour deposition of thin ZnO films.[2] Further studies on these benchmark systems showed that they are amenable to transamination reactions [8] and exchange of the carboxyl groups (as evidenced by $^{13}CO_2$ uptake).[9] The complex $[Al_4(\mu_3\text{-}O)_2(O_2CN i\text{Pr}_2)_8]$ is an example for a tetranuclear carbamate with two oxide ions in its center.[10] Dell'Amico et al. reported on the reaction between a tetranuclear carbamato complex of Ce^{III}, $Ce_4(O_2CN i\text{Pr}_2)_{12}$, and O_2 leading to the product $Ce_4(\mu_3\text{-}O)_2(O_2CN i\text{Pr}_2)_{12}$.[11] This is up to now the only example in which partial oxidation of a carbamate complex with O_2 is reported. Examples of hexanuclear carbamate complexes include $[Co_6(O_2CNEt_2)_{12}]$[12] and $Mn_nMg_{6-n}(O_2CNEt_2)_{12}$ (n = 1–6),[13] and examples for structurally characterized octanuclear carbamate complexes comprise $[Zn_8(\mu_4\text{-}O)_2(O_2CN i\text{Pr}_2)_{12}]$,[14] $[Co_8(\mu_4\text{-}O)_2(O_2CN i\text{Pr}_2)_{12}]$,[15] $[Fe_8(\mu_4\text{-}O)_2(O_2CN i\text{Pr}_2)_{12}]$,[16] $[Zn_2Ni_6(\mu_4\text{-}O)_2(O_2CN i\text{Pr}_2)_{12}]$,[17] and $[Zn_{8-n}Mg_n(\mu_4\text{-}O)_2(O_2CN i\text{Pr}_2)_{12}]$ (n = 0.62).[18]

Tetranuclear Zn carbamate complexes of the form $[ZnR(O_2CNR'_2)]_4$ (R, R′ = alkyl) are the products of reaction between $RZnNR'_2$ (or ZnR_2/HNR'_2 mixtures) and CO_2.[3,19,20] We recently reported on the thermal decomposition of the tetranuclear Zn carbamate complexes $[ZnEt(O_2CNR_2)]_4$ (R = *i*Pr or *i*Bu) leading at relatively mild conditions (200 °C) to ZnO nanoparticles.[3] It was also shown that the tetrameric structure can be split by the action of the N-base pyridine into dimeric units.[21,22] We reported on the first monomeric Zn complex featuring κ^1-coordinated carbamato ligands, namely $[(tmg)_2Zn(O_2CN(i\text{Bu})_2)_2]$ by reaction between $[ZnEt(O_2CN(i\text{Bu})_2)]_4$ and four or more equivalents of tetramethylguanidine (tmg).[24] We also showed that reaction of $[ZnEt(O_2CN(i\text{Pr})_2)]_4$ with only two equivalents of tmg leads to the binuclear complex $[(tmg)ZnEt(O_2CN(i\text{Pr})_2)]_2$.[22] The product of the reaction between $[ZnEt(O_2CNR_2)]_4$ and four equivalents of btmgn (1,8-bis(tetramethylguanidino)naphthalene) turned out to be the mononuclear complex $[(btmgn)ZnEt(O_2CN(i\text{Pr})_2)]$, again with a κ^1-coordinated carbamato ligand. Finally, if only two equivalents are used, the trinuclear complex $[(btmgn)Zn_3Et_3(O_2CN(i\text{Pr})_2)_3]$ is formed.[25] These results

[a] Anorganisch-Chemisches Institut, Ruprecht-Karls-Universität Heidelberg,
Im Neuenheimer Feld 270, 69120 Heidelberg, Germany
Fax: +49-6221-545707
E-mail: hans-jorg.himmel@aci.uni-heidelberg.de
[b] Institut für Katalyseforschung und -technologie,
Karlsruher Institut für Technologie (KIT), Campus Nord,
Postfach 3640, 76021 Karlsruhe, Germany
Supporting information for this article is available on the WWW under http://dx.doi.org/10.1002/ejic.201100019.

motivated us to find ways to break up the tetranuclear carbamato complex by an N-base which itself is attached to a transition metal complex of a different late-transition metal in the formal oxidation state +II. By this means it should be possible to cleave the complex and at the same time introduce a second metal. Herein we report on the synthesis of a new octanuclear Mn_6Zn_2 carbamate complex using this new synthetic approach to heterobimetallic carbamato complexes. The complex exhibits a central empty void. Oxidation with O_2 leads to the filling of the void with one oxygen. The carbamate complex will be shown to be a precursor for the formation of Zn/Mn oxide nanoparticles under mild conditions.

Results and Discussion

Synthesis and Characterization of the New Mn_6Zn_2 Carbamate

As already mentioned, we studied recently the fragmentation of the tetranuclear Zn carbamate complex $[ZnEt(O_2CNR_2)]_4$ (R = *i*Pr or *i*Bu) by N-bases.[25] Motivated by these studies, we tried to synthesize new mixed carbamates by reaction of this tetramer with a transition metal complex to which ligands with secondary amino groups are attached. The base fulfils two tasks: first it should break up the tetrameric unit, and secondly it should provide protons for ethane abstraction. We therefore synthesized three Mn^{II} dichloride complexes, containing as ligands the bases pyridine (py), 2-(methylamino)pyridine (mapy), or 2-[2-(methylamino)ethyl]pyridine (maepy), see Scheme 1. The complexes were generally used immediately after their preparation without isolation. However, in the case of py and maepy, we obtained crystal structures. Of these, the structure of $[(py)_2MnCl_2]$ in the solid state was already determined previously and shown to consist of linear chains of octahedrally coordinated Mn^{II} centers, in which all chlorides adopt bridging positions.[23] On the other hand, the structure of the complex $[(maepy)MnCl_2]$ was previously unknown. It was crystallized from methanol solutions, providing crystals suitable for an XRD analysis (see Figure 1). Again octahedral coordination is achieved, and both the pyridine N as well as the amino N atoms are bound to the Mn^{II} centers. Linear chains result as depicted in Figure 1. The Mn–Cl distances cover the range 253–261 pm, and the closest Mn···Mn separations amount to 379.6(3) pm. In the case of mapy, no crystal formation was monitored.

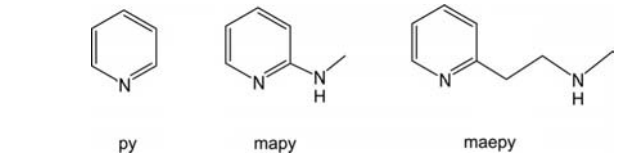

Scheme 1.

THF solutions of each of the three Mn complexes, formed from manganese dichloride and the ligand, were directly brought to reaction with a toluene solution of the zinc carbamate $[ZnEt(O_2CN(iPr)_2)]_4$. In the case of the ligands py and maepy, the experiments gave no evidence for the formation of a mixed metal carbamate. On the other hand, reaction between $[ZnEt(O_2CN(iPr)_2)]_4$ and $[(mapy)MnCl_2]$ resulted in a solid product which was recrystallized from toluene to give colourless crystals of the octanuclear mixed metal carbamate $[Zn_2Mn_6(\mu_4\text{-}O)_2(O_2CN(iPr)_2)_{12}]$ (toluene solvate). The molecular structure as derived from an XRD analysis of the crystalline material is visualized in Figure 2. The molecules possess crystallographic C_2 symmetry. The six Mn atoms are arranged in the form of a highly distorted trigonal antiprism. The trigonal faces are capped by OZn units. Three carbamate ligands on each side of the complex connect the Zn^{II} with the Mn^{II} atoms in a μ_2 bonding mode. The two trigonal Mn_3 units of the central trigonal antiprism are connected by additional six carbamate ligands with a μ_3 bonding mode. One of the carbamate oxygen atoms is bound to only one manganese ion, while the other carbamate oxygen is bound to one manganese ion of the same trigonal face and in addition to one manganese ion from the other trigonal face of the Mn_6 trigonal antiprism. The molecular structure thus resembles the structures of the previously characterized octanuclear carbamate complexes $[Zn_8(\mu_4\text{-}O)_2(O_2CN(iPr)_2)_{12}]$,[16]

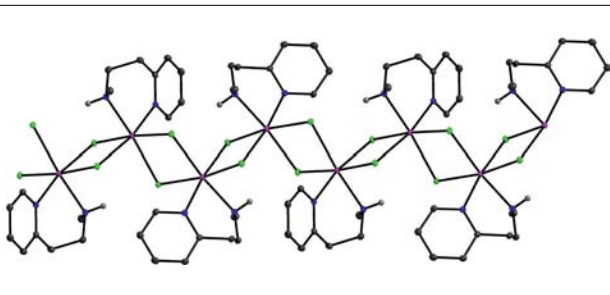

Figure 1. Section of the polymeric structure of $[(mapy)MnCl_2]$ in the crystalline state. Vibrational ellipsoids are drawn at the 50% probability level. Hydrogen atoms bound to carbon atoms were omitted for sake of clarity. Colour code: Mn purple, N blue, C dark grey.

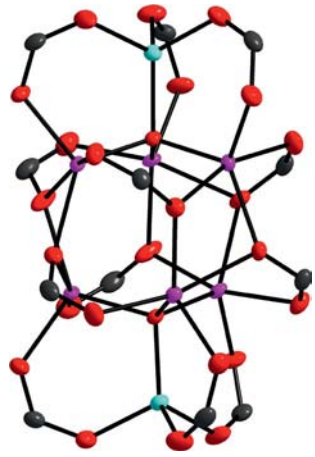

Figure 2. Molecular structure of the octanuclear carbamate complex $[Zn_2Mn_6(\mu_4\text{-}O)_2(O_2CN(iPr)_2)_{12}]$. Vibrational ellipsoids are drawn at the 50% probability level. The amino groups ($NiPr_2$) of the carbamato ligands were omitted for sake of clarity. Colour code: Mn purple, Zn cyan, N blue, C dark grey.

$[Co_8(\mu_4\text{-}O)_2(O_2CN(i\text{Pr})_2)_{12}]$,[17] $[Fe_8(\mu_4\text{-}O)_2(O_2CN(i\text{Pr})_2)_{12}]$,[18] $[Zn_2Ni_6(\mu_4\text{-}O)_2(O_2CN(i\text{Pr})_2)_{12}]$,[19] and $[Zn_{8-n}Mg_n(\mu_4\text{-}O_2)(O_2CN(i\text{Pr})_2)_2]_{12}$ (n = 0.62).[20] The UV/Vis spectrum of $[Zn_2Mn_6(\mu_4\text{-}O)_2(O_2CN(i\text{Pr})_2)_{12}]$ in a $CHCl_3$ solution is shown in Figure 3 (a). It contains relatively weak absorptions centered near 238 and 301 nm. The magnetic curve derived from SQUID measurements is presented in Figure 3 (b). At 300 K, the χT value was found to be 15.6 K cm^3 mol^{-1}. In the absence of magnetic coupling between the Mn^{II} centers and high-spin configuration of each Mn^{II} (S = 5/2), the maximum: χT value for the 6×5 spins can be estimated to be 26.26 K cm^3 mol^{-1} (if g = 2 and spin-orbit coupling can be neglected). As anticipated, antiferromagnetic coupling between the spin centers reduces the χT value considerably. The behaviour at lower temperatures is in line with antiferromagnetic coupling resulting in a singlet ground electronic state. EPR spectra of the complex are provided in the Supporting Information. They show a relatively broad signal with no fine structure, and are similar to the spectra reported for the Mn carbamate $[Mn_6(O_2CNEt_2)_{12}]$.[15]

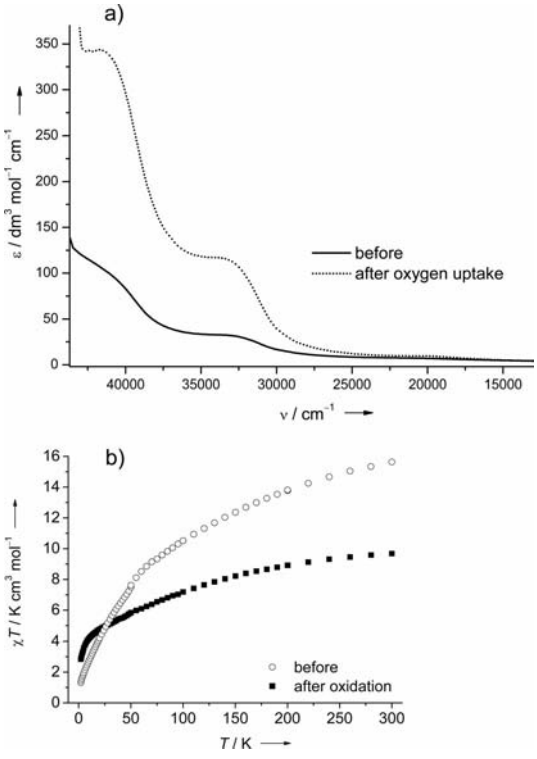

Figure 3. a) UV/Vis spectra in $CHCl_3$ solutions; and b) χT vs. T plots from SQUID measurements (at 500 Oe) of the solid compound as recorded for the carbamate complexes $Zn_2Mn_6(\mu_4\text{-}O)_2(O_2CN(i\text{Pr})_2)_{12}]$ and $[Zn_2Mn_6(\mu_4\text{-}O)_2(\mu_3\text{-}O)(O_2CN(i\text{Pr})_2)_{12}]$.

Generally, the μ_4-O atoms in carbamate complexes arise from water which is added after carbamate formation to the solution. For example, $[Zn_4(\mu_4\text{-}O)(O_2CNEt_2)_6]$ was prepared by addition of H_2O to a reaction mixture of $ZnEt_2$, $HNEt_2$ and CO_2.[16] In our case, we did not add any extra water at the end of the synthesis of $[Zn_2Mn_6(\mu_4\text{-}O)_2(O_2CN(i\text{Pr})_2)_{12}]$. The water needed to form the complex is already initially coordinated to the manganese dichloride, which was used in the overall formula $MnCl_2{\cdot}0.22H_2O$. TG measurements confirmed this $MnCl_2/H_2O$ ratio (see Supporting Information). The coordinated water can also be clearly seen in the IR spectra (see also Supporting Information).[24] The amount of water is critical, and a larger excess of it reduces the yield. Hence when we increased the $MnCl_2/H_2O$ ratio further to 1:2 by addition of extra water to a mixture of the manganese dichloride, mapy, and $[ZnEt(O_2CN(i\text{Pr})_2)]_4$ (see Exp. Section), we only isolated crystals of the salt $[(mapy)H]^+[(mapy)ZnCl_3]^-$ (see Supporting Information) from the reaction mixture.

Oxygen Uptake

When a solution of the carbamate $[Zn_2Mn_6(\mu_4\text{-}O)_2(O_2CN(i\text{Pr})_2)_{12}]$ was stirred under air, a colouring of the solution signals (partial) Mn^{II} oxidation. First information about the product was derived from mass spectrometric data. Figure 4 (a) shows the M^+ peak region of the mass spectrum recorded after 15 min air expose of a $[Zn_2Mn_6(\mu_4\text{-}O)_2(O_2CN(i\text{Pr})_2)_{12}]$ solution. The isotopic pattern fits nicely to the simulated pattern. In addition, a peak appears which can be explained by the uptake of one oxygen atom. After completion of this oxidation process, the peak due to $[Zn_2Mn_6(\mu_4\text{-}O)_2(O_2CN(i\text{Pr})_2)_{12}]$ almost completely disappeared (see Figure 4, b). The spectrum provided in Figure S3 of the Supporting Information also indicates that at this stage no product with two or more additional oxygen atoms is formed. It proved possible to crystallize the oxidation product as a toluene solvate, and Figure 5 shows its molecular structure. The molecules are centrosymmetric. The void of the carbamate is now filled with one oxygen atom, leading to the formula $[Zn_2Mn_6(\mu_4\text{-}O)_2(\mu_3\text{-}O)(O_2CN(i\text{Pr})_2)_{12}]$. The oxygen atom occupies two different sites (separated by 80.1(1) pm) in this void. Three of the six Mn atoms become sixfold coordinated by oxygen [distorted octahedral coordination mode, with Mn–O distances of 208.1(9), 226(1) and 239(1) pm]. The three remaining Mn···O separations amount to 247(1), 261(1) and 271(2) pm. The six Mn atoms are now clearly arranged in the form of a trigonal antiprism. The six carbamate ligands bridging the two trigonal faces still adopt a μ_3-bonding mode. However, one of the carbamate oxygen atoms is now bound to two Mn centers of the same trigonal face of this antiprism, while the other oxygen atom is bound to only one Mn ion of the other trigonal face. This change in the carbamate bonding mode relative to the situation before oxidation increases the size of the cage within the complex. Figure 5 also illustrates the packing of the molecules in the crystalline state, showing that all complexes are lined up. With 885.8(2) pm, the shortest intermolecular Zn···Zn separations are shorter than the intramolecular Zn···Zn separation of 889.0(2) pm. The UV/Vis spectra recorded for $[Zn_2Mn_6(\mu_4\text{-}O)_2(\mu_3\text{-}O)(O_2CN(i\text{Pr})_2)_{12}]$ is compared to that of the initial $[Zn_2Mn_6(\mu_4\text{-}O)_2(O_2CN(i\text{Pr})_2)_{12}]$ complex in Figure 3 (a). The main difference between the spectra before and after oxidation is

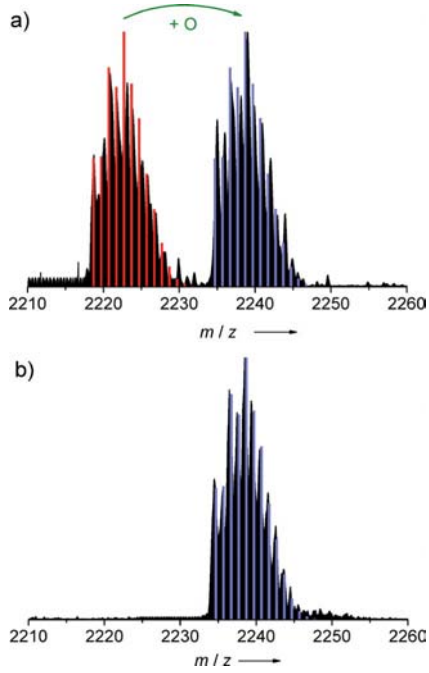

Figure 4. Mass spectrometry of the carbamate complexes. a) mixture of non-oxidized and oxidized carbamate obtained upon exposure of $Zn_2Mn_6(\mu_4\text{-}O)_2(O_2CN(i\text{Pr})_2)_{12}$] to air for a period of 15 min. b) The oxidized carbamate [$Zn_2Mn_6(\mu_4\text{-}O)_2(\mu_3\text{-}O)(O_2CN(i\text{Pr})_2)_{12}$].

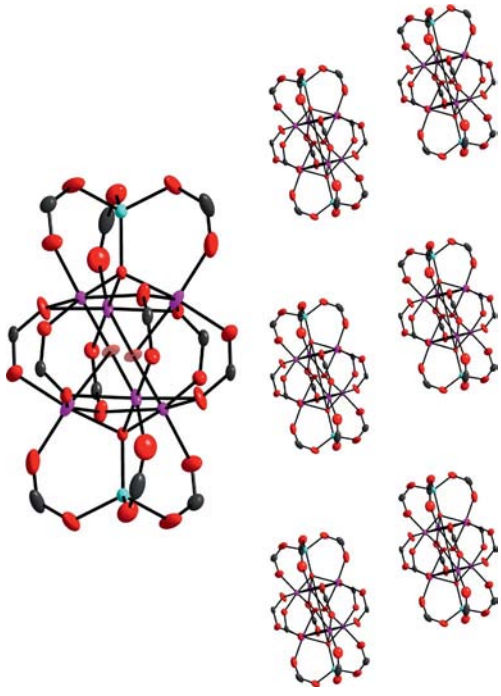

Figure 5. Molecular structure of the octanuclear carbamate complex [$Zn_2Mn_6(\mu_4\text{-}O)_2(\mu_3\text{-}O)(O_2CN(i\text{Pr})_2)_{12}$]. Vibrational ellipsoids are drawn at the 50% probability level. The amino groups ($NiPr_2$) of the carbamato ligands were omitted for sake of clarity. The μ_3-O (pale colour) is distributed equally over two sites within the central cage. The packing of the molecules in the crystalline material is also shown. Colour code: Mn purple, Zn cyan, N blue, C dark grey.

the increase of the extinction coefficient upon oxidation. The wavenumbers of the absorption maxima (294 and 232 nm) are virtually unchanged. The $\chi T-T$ curve for [$Zn_2Mn_6(\mu_4\text{-}O)_2(\mu_3\text{-}O)(O_2CN(i\text{Pr})_2)_{12}$] as derived from SQUID measurements is presented in part b of Figure 3. As anticipated (simply on the basis of the reduced number of unpaired electrons), the χT value at room temperature (9.7 $K\,cm^3\,mol^{-1}$) is smaller than that of the complex before oxidation (15.6 $K\,cm^3\,mol^{-1}$).

It should be noted that the carbamate [$Zn_2Mn_6(\mu_4\text{-}O)_2(\mu_3\text{-}O)(O_2CN(i\text{Pr})_2)_{12}$] is not formed if pure O_2 is bubbled (for 20 min) through a toluene solution of [$Zn_2Mn_6(\mu_4\text{-}O)_2(O_2CN(i\text{Pr})_2)_{12}$]. Instead, we observed in this case decomposition and further oxidation of manganese to give MnO_2. The [$Zn_2Mn_6(\mu_4\text{-}O)_2(\mu_3\text{-}O)(O_2CN(i\text{Pr})_2)_{12}$] complex also is oxidized further to give MnO_2 if pure O_2 is used as reactant. Thus [$Zn_2Mn_6(\mu_4\text{-}O)_2(\mu_3\text{-}O)(O_2CN(i\text{Pr})_2)_{12}$] most likely represents only an intermediate of the oxidation process.

Thermal Stability and Decomposition to Magnetic Oxides

In line with other carbamates,[3] decomposition of [$Zn_2Mn_6(\mu_4\text{-}O)_2(O_2CN(i\text{Pr})_2)_{12}$] occurs already at mild conditions. Figure 6 shows the TG curves for three different heating rates (2, 5 and 10 °C min^{-1}). For all heating rates, the complex witnesses a similar loss of ca. 73% of its initial mass. This fits nicely to the theoretical mass loss of 74% for decomposition to give an oxide of the overall formula $ZnMn_3O_4$. The decomposition is completed at 210 °C for a heating rate of 2 °C min^{-1}, but requires temperatures of more than 270 °C if the heating rate is increased to 10 °C min^{-1}. This behaviour indicates kinetic control of the decomposition for high heating rates implying that decomposition is a relatively slow process. A similar behaviour was observed for decomposition of [$ZnEt(O_2CN(i\text{Pr})_2)]_4$ to give ZnO.[3] The decomposition product appears almost black. For comparison, ZnO doped with Mn (as often the case in the naturally occurring mineral zincite)[25] is red-coloured. The potential to use Mn doped ZnO as red pigment was recently evaluated in detail.[26] In this study, the $Zn_{1-x}Mn_xO$ samples ($x \leq 0.17$) were synthesized from ZnO and MnO in

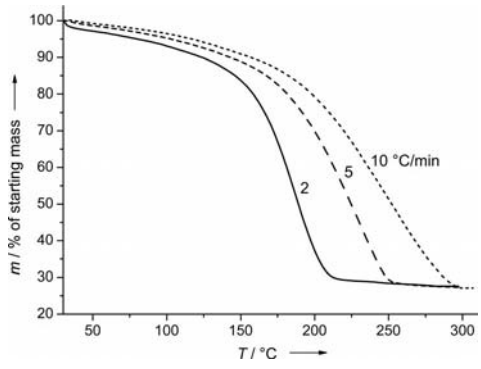

Figure 6. TG curves recorded for [$Zn_2Mn_6(\mu_4\text{-}O)_2(O_2CN(i\text{Pr})_2)_{12}$] at three different heating rates (2, 5 and 10 °C min^{-1}).

the presence of NH_4Cl at 850 °C. In our case, the dark colour of the product points to formation of a different oxide, in line with the high Mn content in the precursor.

Further information was obtained from X-ray powder diffraction data (for a heating rate of 5 K min^{-1}). Figure 7 displays a typical diffraction pattern, which cannot be explained by a single phase, but with respect to the results from the EDX analyses rather points to formation of $ZnMn_2O_4$ and MnO nanoparticles. For comparison, the characteristic lines of these two lattices are included in Figure 7. No additional amorphous particles are formed. A Debye–Scherer analysis to estimate the particle sizes proved impossible due to peak overlapping. However, from the powder pattern it can be derived that the particles have to be small as otherwise sharper peaks would have been observed in the diffractogramms. These findings are supported by the results of a TEM analyses (see Figure 7 and Supporting Information) showing that the particle size is ≤23 nm (mean particle size of 9 nm). EDX measurements at different places of the sample (see Supporting Information) show slight variations in the Mn/Zn ratio, which in average amounts to ca. 3:1, in line with the other analytical data.

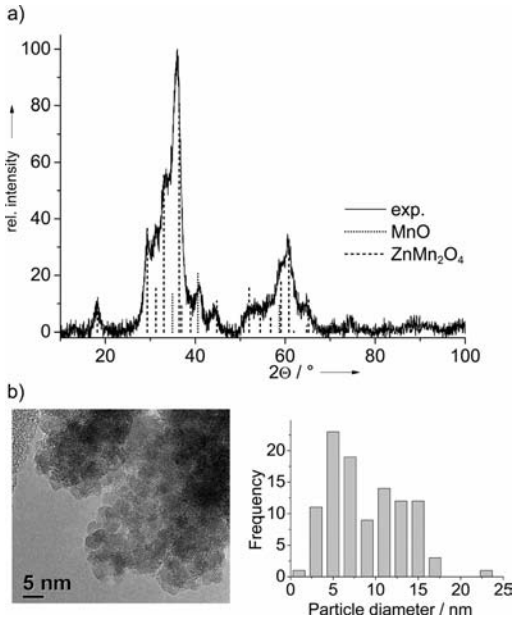

Figure 7. a) Powder diffractogramm, and b) TEM image with particle size distribution (mean particle diameter 8.8 ± 4.3 nm) obtained after thermal decomposition of $[Zn_2Mn_6(\mu_4\text{-}O)_2(O_2CN(i\text{Pr})_2)_{12}]$ (end temperature 300 °C, 5 °C min^{-1} heating rate).

The TG curves recorded for $[Zn_2Mn_6(\mu_4\text{-}O)_2(\mu_3\text{-}O)(O_2CN(i\text{Pr})_2)_{12}]$ are similar to those of $[Zn_2Mn_6(\mu_4\text{-}O)_2(O_2CN(i\text{Pr})_2)_{12}]$, showing the same dependence of the final temperature for complete decomposition on the heating rate. Again, the XRD data (see Supporting Information) showed the presence of crystalline $ZnMn_2O_4$ and MnO nanoparticles. An analysis of the TEM pictures (see Supporting Information) might indicate a slightly narrower particle size distribution.

Quantum Chemical Calculations

Calculations were carried out using the BP functional in combination with a def2-SV(P) basis set. The carbamate $[Zn_2Mn_6(\mu_4\text{-}O)_2(O_2CN(i\text{Pr})_2)_{12}]$ features six Mn^{II} centers each with five unpaired electrons, yielding in total 30 unpaired electrons. The oxidized carbamate $[Zn_2Mn_6(\mu_4\text{-}O)_2(\mu_3\text{-}O)(O_2CN(i\text{Pr})_2)_{12}]$ contains four Mn^{II} and two Mn^{III} centers yielding 28 unpaired electrons. Owing to magnetic coupling between the different centers a large number of electronic states with small energy separations is expected. For simplification we only considered high-spin terms and also replaced the *i*Pr groups by hydrogen atoms. Thus the calculations assume a ^{31}A term for $[Zn_2Mn_6(\mu_4\text{-}O)_2(O_2CNH_2)_{12}]$, and a ^{29}A term for $[Zn_2Mn_6(\mu_4\text{-}O)_2(\mu_3\text{-}O)(O_2CNH_2)_{12}]$. They especially addressed the following points: 1) Search for other possible energy minima and the activation barrier for conversions from one minimum to the other for oxygen in the void. 2) The thermodynamic properties for O_2 uptake.

The minimum energy structure of $[Zn_2Mn_6(\mu_4\text{-}O)_2(O_2CNH_2)_{12}]$ turned out to exhibit D_3 symmetry. In the case of the oxidized complex $[Zn_2Mn_6(\mu_4\text{-}O)_2(\mu_3\text{-}O)(O_2CNH_2)_{12}]$, two different kinds of C_1 symmetric structures resulted, in which the additional O atom within the Mn_6 void is bound to three Mn atoms (with Mn–O distances of about 200 pm) and exhibits longer O···Mn separations to the three remaining Mn atoms of ca. 300 pm. For each of the two kinds of minima, there exist six identical structures on the hypersurface that result from binding the oxygen atom to six different but symmetry equivalent sites within the D_3 symmetric structure of the $[Zn_2Mn_6(\mu_4\text{-}O)_2(O_2CNH_2)_{12}]$ complex. The two different kinds of minima differ in the location of the Mn^{III} centers, given the O atom is bound to the same three Mn atoms, see Min1′ and Min2 in Figure 8. (The short Mn–O distances indicate the Mn^{III} centers.) The energy difference between the structures amounts to 0.3 kJ mol^{-1} only, Min1′ being the lower one.

Furthermore, a transition structure was calculated that separates two minimum structures of different kind with the oxygen at adjacent sites. Those two structures share the location of the Mn^{III} centers, i.e. within both structures, the Mn^{III} oxidation state is attributed to the same Mn atoms and the motion corresponds to a simple oxygen shift. Within this transition structure (C_1 symmetry), the central O atom is bound to two Mn atoms with relatively short distances (189.2 and 192.3 pm), and to two further Mn atoms with much longer distances of 240.2 and 275.2 (see Figure 8). According to the calculations, the energy of the transition state lies only 0.8 kJ mol^{-1} higher than that of the lower minimum structure. Thus a barrier less than 1 kJ mol^{-1} separates the two minima.

For a free relocation of the oxygen within the cage via the calculated transition structure two steps are necessary: (a) the transfer of the O atom to an adjacent place and (b) the interchange of the oxidation states of a Mn^{II}/Mn^{III} pair. Unfortunately, the transition structure for the second step is hard to obtain, because different electronic configurations

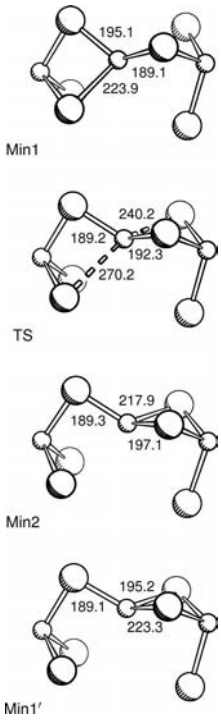

Figure 8. Calculated structure of two different minima (Min1 and Min2) and a relating transition structure of $[Zn_2Mn_6(\mu_4\text{-}O)_2(\mu_3\text{-}O)(O_2CNH_2)_{12}]$. In addition, a further minimum Min1′ equivalent to Min1 is shown. Min2 and Min1′ can be interconverted by single electron transfer between two M atoms. The calculations relied on the BP functional and a SV(P) basis set.

associated with the different oxidation states are involved, and therefore the determination of the barrier for oxidation state interchange demands a multireference treatment. For the given system the effort would be to large to get results in a reasonable time scale, and therefore a value for the effective barrier of the oxygen movement cannot be provided.

In any case, since the movement is accompanied by a change in the coordination sphere and since packing effects are likely to reduce the flexibility of the complex, the free movement is probably restricted within the crystalline phase. Apparently, the shape of the complex allows the statistical packing of complexes with two orientations. The calculated dipole moment for $[Zn_2Mn_6(\mu_4\text{-}O)_2(\mu_3\text{-}O)(O_2CN(i\text{Pr})_2)_{12}]$ amounts to ca. 0.83 debye. On the basis of these calculations and the favourable packing of the molecules in the crystal (see Figure 5), it might be possible to orientate the individual dipole moments by an external electric field (ferroelectric behaviour).

For both the oxidized and the reduced form of the complex, vibrational spectra have been calculated and they turn out to be very similar (see Supporting Information), which is also the case for the observed spectra. The calculations estimate the reaction of $[Zn_2Mn_6(\mu_4\text{-}O)_2(O_2CNH_2)_{12}]$ with 1/2 O_2 to give $[Zn_2Mn_6(\mu_4\text{-}O)_2(\mu_3\text{-}O)(O_2CNH_2)_{12}]$ to be accompanied by a reaction enthalpy $\Delta_R H$ (0 K) (only electronic contribution) of –454.1 kJ mol^{-1}. In the case of reaction between $[Zn_2Mn_6(\mu_4\text{-}O)_2(O_2CNH_2)_{12}]$ and H_2O to give $[Zn_2Mn_6(\mu_4\text{-}O)_2(\mu_3\text{-}O)(O_2CNH_2)_{12}]$ and H_2, the reaction enthalpy $\Delta_R H$ (0 K) is –86.3 kJ mol^{-1}.

Conclusions

Herein we presented a new method for the preparation of heterobimetallic carbamates, which we applied exemplarily for the formation of Mn/Zn carbamates. It starts with an alkylzinc carbamate $[ZnR(O_2CNR'_2)]_4$ (R = Et, R′ = *i*Pr), which is brought to reaction with a manganese dichloride complex featuring a pyridine ligand to which a secondary amine unit is attached. This amine unit fulfils two tasks: it splits up the tetrameric Zn carbamate and provides protons for alkane elimination. In this way we synthesized the octanuclear carbamate complex $[Zn_2Mn_6(\mu_4\text{-}O)_2(O_2CN(i\text{Pr})_2)_{12}]$. We are currently evaluating the synthesis of Co/Zn carbamates using a similar route, and preliminary results show that indeed new heterobimetallic carbamates can be formed also in this case.[27] These heterobimetallic carbamates can be used for the synthesis of mixed metal oxide nanoparticles by decomposition of the carbamates under mild conditions (210–270 °C). A mixture of $ZnMn_2O_4$ and MnO nanoparticles is produced. Nanocrystalline $ZnMn_2O_4$ (spinel structure) is of considerable interest for several applications, e.g. as a novel lithium-storage material.[28] Its fabrication by polymer-pyrolysis methods needs much higher temperatures (pyrolysis step at 600 °C) than the procedure described herein.

The $[Zn_2Mn_6(\mu_4\text{-}O)_2(O_2CN(i\text{Pr})_2)_{12}]$ complex turned out to be extremely oxidation sensitive. Hence reaction with O_2 yields the new carbamate complex $[Zn_2Mn_6(\mu_4\text{-}O)_2(\mu_3\text{-}O)(O_2CN(i\text{Pr})_2)_{12}]$ (as first isolated intermediate on the way to MnO_2 formation). In this complex, the empty void within the carbamate complex is filled with one oxygen atom, which in the crystalline material is equally distributed over two sites. The void is increased relative to the situation before oxidation by a change in the carbamate bonding mode.

Experimental Section

General: All reactions were carried out using standard Schlenk technique under an atmosphere of N_2. All solvents were dried prior to their use. UV/Vis spectra were taken with a Varian CARY 5000 spectrometer. For the SQUID direct current (dc) measurements, a Quantum Design MPMS-XL 5 machine was used. EPR measurements relied on a Bruker Elexsys E500 spectrometer. Positive field desorption (FD^+) mass spectrometric measurements were taken on a JeolJMS mass spectrometer. Elemental analyses were carried out at the Microanalytical Laboratory of the University of Heidelberg. IR spectra were recorded on a Biorad Excalibur FTS3000 spectrometer. Thermogravimetric (TG) measurements were carried out on a Mettler TC15 under Ar atmosphere in a temperature range 30–600 °C. The heating rate was varied between 2 and 10 K/min. TEM experiments were performed with a FEI Tecnai F20 TEM [equipped with an energy dispersive X-ray (EDX) spectrometer] with field emission gun at 200 kV on carbon-coated 400 mesh cop-

per grids. The XRD measurements were performed on a STADI P machine from STOE and a Siemens D500 diffractometer using Cu radiation. The data were evaluated with EVA (DIFFRACplus, EVA 9.0, XRD evaluation programme, Bruker AXS, 2003).

$[Mn_6Zn_2(\mu_4\text{-}O)_2(O_2CN(i\text{Pr})_2)_{12}]$: 2-(Methylamino)pyridine (mapy) (0.440 g, 4.06 mmol) was added to a THF (10 mL) suspension of $MnCl_2{\cdot}0.22H_2O$ (0.255 g, 1.96 mmol). The clear reaction mixture was stirred at room temp. for a period of 1 h. Upon addition of a toluene solution (10 mL) of $[EtZn(O_2CN(i\text{Pr})_2)]_4$ (1 g, 1.02 mmol), the reaction mixture turned to a yellow colour. It was stirred at room temp. for 72 h and then evaporated to dryness. Recrystallization of the solid product from toluene at room temp. yielded colourless crystals of the product (0.21 g, 0.094 mmol, 27.8%). $C_{84}H_{168}Mn_6N_{12}O_{26}Zn_2{\cdot}C_7H_8$(toluene) (2313.81): calcd. C 47.19, H 7.62, N 7.26; found C 47.33, H 7.62, N 7.46. IR (CsI): 1566, 1450 [ν(CO)] cm^{-1}. UV/Vis ($CHCl_3$, $c = 3.10\times10^{-3}$ mol·L^{-1}): 33112 cm^{-1} (301 nm, ε = 32 $dm^3mol^{-1}cm^{-1}$), 42016 cm^{-1} (238 nm, ε = 110 $dm^3mol^{-1}cm^{-1}$). UV/Vis (CH_3CN, $c = 2.6\times10^{-3}$ mol·L^{-1}): 33112 cm^{-1} (301 nm, ε = 54 $dm^3mol^{-1}cm^{-1}$), 41322 cm^{-1} (238 nm, ε = 113 $dm^3mol^{-1}cm^{-1}$). UV (solid): λ_{max} = 314, 238 nm. MS(FD^+) calcd. 2222.70; found 2222.72. Crystal data for $[Mn_6Zn_2(\mu_4\text{-}O)_2(O_2CN(i\text{Pr})_2)_{12}]{\cdot}$toluene, $C_{91}H_{175}Mn_6N_{12}O_{26}Zn_2$, M_r = 2313.81, $0.22\times0.18\times0.16$ mm^3, orthorhombic, space group *Pbcn*, a = 22.466(11) Å, b = 23.113(12) Å, c = 23.385(11) Å, V = 12143(11) $Å^3$, Z = 4, $d_{calcd.}$ = 1.266 $Mg\,m^{-3}$, Mo-K_α radiation (graphite-monochromated, λ = 0.71073 Å), T = 100 K, θ_{range} 1.74 to 30.03°. Reflections measured 289662, independent 17779, R_{int} = 0.0661. Final R indices [$I>2\sigma(I)$]: R_1 = 0.0516, wR_2 = 0.1308.

$[Mn_6Zn_2(\mu_4\text{-}O)_2(\mu_3\text{-}O)(O_2CN(i\text{Pr})_2)_{12}]$: A toluene solution (5 mL) of $[Zn_2Mn_6(\mu_4\text{-}O)_2(O_2CN(i\text{Pr})_2)_{12}]$ (0.0231 g, 0.01 mmol) was stirred for 48 h at room temp. (allowing a few air contacts) during which time the reaction mixture changes the colour from colourless to brown. The solution was then evaporated to dryness. The solid product was recrystallized from toluene/hexane, 4:1 at room temperature to give brown crystals (0.0224 g, 0.0097 mmol, 97%). $C_{84}H_{168}Mn_6N_{12}O_{27}Zn_2{\cdot}C_7H_8$(toluene) (2329.81): calcd. C 46.33, H 7.61, N 7.21; found C 47.07, H 7.71, N 7.46. IR (CsI): 1566, 1466 [ν(CO)] cm^{-1}. UV/Vis ($CHCl_3$, $c = 3.10\times10^{-3}$ mol·L^{-1}): 34013 cm^{-1} (294 nm, ε = 114 $dm^3mol^{-1}cm^{-1}$), 43103 cm^{-1} (232 nm, ε = 376 $dm^3mol^{-1}cm^{-1}$). UV (solid): λ_{max} = 500, 288, 244 nm. MS(FD^+) calcd. 2238.69; found 2238.53. Crystal data for $[Mn_6Zn_2(\mu_4\text{-}O)_2(\mu_3\text{-}O)(O_2CN(i\text{Pr})_2)_{12}]{\cdot}$toluene, $C_{91}H_{175}Mn_6N_{12}O_{27}Zn_2$, M_r = 2329.81, $0.12\times0.12\times0.06$ mm^3, triclinic, space group $P\bar{1}$, a = 14.776(7) Å, b = 14.852(8) Å, c = 17.114(8) Å, α = 74.003(13)°, β = 66.337(10)°, γ = 60.644(8)°, V = 2984(3) $Å^3$, Z = 1, $d_{calcd.}$ = 1.297 $Mg\,m^{-3}$, Mo-K_α radiation (graphite-monochromated, λ = 0.71073 Å), T = 100 K, θ_{range} 1.71 to 25.03°. Reflections measured 50334, independent 10543, R_{int} = 0.076. Final R indices [$I>2\sigma(I)$]: R_1 = 0.0567, wR_2 = 0.1341.

Preparation of Zn/Mn Heterobimetallic Nanoparticles Starting with $[Mn_6Zn_2(\mu_4\text{-}O)_2(O_2CN(i\text{Pr})_2)_{12}]$: The carbamate precursor $[Mn_6Zn_2(\mu_4\text{-}O)_2(O_2CN(i\text{Pr})_2)_{12}]$ (0.012 g, 0.005 mmol) was filled in a platinum crucible. The compound was heated with a heating rate of 5 °C min^{-1} (for the TG analysis also heatig rates of 2 and 10 °C min^{-1} were used) to an end temperature of 300 °C under a nitrogen atmosphere with a flow rate of 150 mL min^{-1}. XRD measurements indicated formation of the oxides $ZnMn_2O_4$ and MnO. The EDX analysis is in line with an overall Mn/Zn ratio of, 3:1. TEM data of 105 particles argue for a mean particle size of 8.8 ± 4.3 nm (minimum: 1.9 nm, maximum: 23.0 nm).

Preparation of Zn/Mn Heterobimetallic Nanoparticles Starting with $[Mn_6Zn_2(\mu_4\text{-}O)_2(\mu_3\text{-}O)(O_2CN(i\text{Pr})_2)_{12}]$: The carbamate precursor $[Mn_6Zn_2(\mu_4\text{-}O)_2(\mu_3\text{-}O)(O_2CN(i\text{Pr})_2)_{12}]$ (0.012 g, 0.005 mmol) was filled in a platinum crucible. The compound was heated with a heating rate of 5 °C min^{-1} (for the TG analysis also heating rates of 2 and 10 °C min^{-1} were used) to an end temperature of 300 °C under a nitrogen atmosphere with a flow rate of 150 mL min^{-1}. XRD measurements indicated formation of the oxides $ZnMn_2O_4$ and MnO. The EDX analysis is in line with an overall Mn/Zn ratio of, 3:1. TEM data of 210 particles argue for a mean particle size of 8.4 ± 3.1 nm (minimum: 2.5 nm, maximum: 18.2 nm).

X-ray Crystallographic Study: Suitable crystals were taken directly out of the mother liquor, immersed in perfluorinated polyether oil, and fixed on top of a glass capillary.

Intensity data were collected at low temperature (100 K) with Nonius Kappa CCD and Bruker AXS Smart 1000 CCD diffractometers (Mo-K_α radiation, graphite monochromator, λ = 0.71073 Å). The data collected were processed using the standard Nonius[29] and Bruker AXS software.[30] The structures were solved by conventional direct methods [31] ([(maepy)$MnCl_2$] and $[(mapy)H]^+[(mapy)ZnCl_3]^-$ (see Supporting Information)) or by the charge flip procedure,[32,33] and refined by full-matrix least-squares methods based on F^2 against all unique reflections.[34] All non-hydrogen atoms were given anisotropic displacement parameters. Hydrogen atoms were put at calculated positions and refined with a riding model. Similarity restraints were used to achieve acceptable geometry of the twelve isopropyl groups (some of which were disordered) in $[Zn_2Mn_6(\mu_4\text{-}O)_2(\mu_3\text{-}O)(O_2CN(i\text{Pr})_2)_{12}]$. Due to severe disorder, electron density attributed to the solvent of crystallization (toluene) was removed from the structure (and the corresponding F_{obs}) of this complex with the BYPASS procedure,[35] as implemented in PLATON (SQUEEZE).[36] The occupancy of the two symmetry equivalent (μ_3-O) positions refined to 0.54(1). In view of the short distance between the two sites their occupancy was constrained to 0.5. Graphical handling of the structural data during solution and refinement was performed with XPMA.[37] Crystal data for [(maepy)$MnCl_2$], $C_{16}H_{24}Cl_4Mn_2N_4$, M_r = 524.07, $0.30\times0.20\times0.15$ mm^3, monoclinic, space group $P2_1/n$, a = 10.971(2) Å, b = 14.929(3) Å, c = 12.844(3) Å, β = 92.39(3)°, V = 2984(3) $Å^3$, Z = 4, $d_{calcd.}$ = 1.656 $Mg\,m^{-3}$, Mo-K_α radiation (graphite-monochromated, λ = 0.71073 Å), T = 100 K, θ_{range} 2.09 to 30.03°. Reflections measured 11840, independent 6131, R_{int} = 0.0174. Final R indices [$I>2\sigma(I)$]: R_1 = 0.0292, wR_2 = 0.0695. Crystal data for $[(mapy)H]^+[(mapy)ZnCl_3]^-$, $C_{12}H_{17}Cl_3N_4Zn$, M_r = 389.02, $0.20\times0.12\times0.12$ mm^3, monoclinic, space group $P2_1/n$, a = 7.4320(15) Å, b = 14.229(3) Å, c = 15.378(3) Å, β = 90.88(3)°, V = 1626.0(6) $Å^3$, Z = 4, $d_{calcd.}$ = 1.589 $Mg\,m^{-3}$, Mo-K_α radiation (graphite-monochromated, λ = 0.71073 Å), T = 100 K, θ_{range} 1.95 to 30.06°. Reflections measured 8934, independent 4739, R_{int} = 0.0417. Final R indices [$I>2\sigma(I)$]: R_1 = 0.0412, wR_2 = 0.0876.

CCDC-793885 (for $[Mn_6Zn_2(\mu_4\text{-}O)_2(O_2CN(i\text{Pr})_2)_{12}]$), -793886 (for $[Zn_2Mn_6(\mu_4\text{-}O)_2(\mu_3\text{-}O)(O_2CN(i\text{Pr})_2)_{12}]$), -793486 (for [(maepy)$MnCl_2$]) and -793487 (for $[(mapy)H]^+[(mapy)ZnCl_3]^-$) contain the supplementary crystallographic data for this paper. These data can be obtained free of charge from The Cambridge Crystallographic Data Centre via www.ccdc.cam.ac.uk/data_request/cif.

Calculational Details: Density functional calculations were performed with the program package TURBOMOLE[38] using the BP functional[39] in combination with the def2-SV(P) basis set.[40] For the numerical integration grid "m4" was used. The two-electron integrals were calculated with the RI approximation.[41] The appropriate auxiliary basis sets were employed.[42]

Supporting Information (see also the footnote on the first page of this article): TG and IR data for the $MnCl_2{\cdot}0.22H_2O$ sample used

in the carbamate preparation, EPR spectra of the carbamate complexes $[Zn_2Mn_6(\mu_4\text{-}O)_2(O_2CN(i\text{Pr})_2)_{12}]$ and $[Zn_2Mn_6(\mu_4\text{-}O)_2(\mu_3\text{-}O)(O_2CN(i\text{Pr})_2)_{12}]$ as well as the oxides resulting from their decomposition, mass spectrometric data for $[Zn_2Mn_6(\mu_4\text{-}O)_2(\mu_3\text{-}O)(O_2CN(i\text{Pr})_2)_{12}]$, IR spectra for $[Zn_2Mn_6(\mu_4\text{-}O)_2(O_2CN(i\text{Pr})_2)_{12}]$ and $[Zn_2Mn_6(\mu_4\text{-}O)_2(\mu_3\text{-}O)(O_2CN(i\text{Pr})_2)_{12}]$, details of the synthesis and structure of $[(mapy)H]^+[(mapy)ZnCl_3]^-$, results of the TEM and EDX measurements, XRD for the oxide particles produced from the precursor $[Zn_2Mn_6(\mu_4\text{-}O)_2(\mu_3\text{-}O)(O_2CN(i\text{Pr})_2)_{12}]$, calculated IR spectra for $[Zn_2Mn_6(\mu_4\text{-}O)_2(O_2CN(i\text{Pr})_2)_{12}]$ and $[Zn_2Mn_6(\mu_4\text{-}O)_2(\mu_3\text{-}O)(O_2CN(i\text{Pr})_2)_{12}]$.

Acknowledgments

The authors gratefully acknowledge continuous financial support from the Deutsche Forschungsgemeinschaft (DFG).

[1] See, for example: a) M. R. Hill, J. Russell, R. N. Lamb, *Chem. Mater.* **2008**, *20*, 2461–2467; M. R. Hill, J. J. Russell, N. K. Roberts, R. N. Lamb, *Polyhedron* **2007**, *26*, 493–507; R. Pothiraja, A. P. Milanov, D. Barreca, A. Gasparotto, H.-W. Becker, M. Winter, R. A. Fischer, A. Devi, *Chem. Commun.* **2009**, 1978–1980.

[2] D. Domide, E. Kaifer, J. Mautz, O. Walter, S. Behrens, H.-J. Himmel, *Eur. J. Inorg. Chem.* **2008**, 3177–3185.

[3] T. C. Taylor, I. Andersson, *Nat. Struct. Biol.* **1996**, *3*, 95–101.

[4] J. L. Vanhooke, M. M. Benning, F. M. Raushel, H. M. Holden, *Biochemistry* **1996**, *35*, 6020–6025.

[5] A. Belforte, F. Calderazzo, U. Englert, J. Strähle, *Inorg. Chem.* **1991**, *30*, 3778–3781.

[6] D. B. Dell'Amico, F. Calderazzo, L. Labella, F. Marchetti, *Inorg. Chim. Acta* **2003**, *350*, 661–664.

[7] M. Casarin, E. Tondello, F. Calderazzo, A. Vittadini, M. Betinelli, A. Gulino, *J. Chem. Soc. Faraday Trans.* **1993**, *89*, 4363–4367.

[8] C. S. McCowan, T. L. Groy, M. T. Caudle, *Inorg. Chem.* **2002**, *41*, 1120–1127.

[9] C. S. McCowan, M. T. Caudle, *Dalton Trans.* **2005**, 238–246.

[10] U. Abram, D. B. Dell'Amico, F. Calderazzo, S. Kaskel, L. Labella, F. Marchetti, R. Rovai, J. Strähle, *Chem. Commun.* **1997**, 1941–1942.

[11] U. Baisch, D. B. Dell'Amico, F. Calderazzo, L. Labella, F. Marchetti, D. Vitali, *J. Mol. Catal. A* **2003**, *204–205*, 259–265.

[12] D. B. Dell'Amico, F. Calderazzo, B. Giovannitti, G. Pelizzi, *J. Chem. Soc., Dalton Trans.* **1984**, 647–652.

[13] M. T. Caudle, C. K. Mobley, L. M. Bafaro, R. LoBrutto, G. T. Yee, T. L. Groy, *Inorg. Chem.* **2004**, *43*, 506–514.

[14] P. F. Haywood, M. R. Hill, N. K. Roberts, D. C. Craig, J. J. Russell, R. N. Lamb, *Eur. J. Inorg. Chem.* **2008**, 2024–2032.

[15] D. B. Dell'Amico, C. Bradicich, F. Calderazzo, A. Guarini, L. Labella, F. Marchetti, A. Tomei, *Inorg. Chem.* **2002**, *41*, 2814–2816.

[16] D. B. Dell'Amico, F. Calderazzo, L. Labella, C. Maichle-Mössmer, J. Strähle, *J. Chem. Soc., Chem. Commun.* **1994**, 1555–1556.

[17] A. Bacchi, D. B. Dell'Amico, F. Calderazzo, U. Giurlani, G. Pelizzi, L. Rocchi, *Gazz. Chim. Ital.* **1992**, *122*, 429–435.

[18] M. R. Hill, P. Jensen, J. J. Russell, R. N. Lamb, *Dalton Trans.* **2008**, 2751–2758.

[19] I. Abrahams, M. A. Malik, M. Motevalli, P. O'Brien, *J. Chem. Soc., Dalton Trans.* **1995**, 1043–1046.

[20] H.-J. Himmel, *Eur. J. Inorg. Chem.* **2007**, 675–683.

[21] C. Neuhäuser, D. Domide, J. Mautz, E. Kaifer, H.-J. Himmel, *Dalton Trans.* **2008**, 1821–1824.

[22] D. Domide, C. Neuhäuser, E. Kaifer, H. Wadepohl, H.-J. Himmel, *Eur. J. Inorg. Chem.* **2009**, 2170–2178.

[23] P. M. Richards, R. K. Quinn, B. Morosin, *J. Chem. Phys.* **1973**, *59*, 4474–4477.

[24] B. K. Srivastawa, D. P. Khandelwal, H. D. Bist, *J. Raman Spectrosc.* **1978**, *7*, 202–204.

[25] E. Dittler, *Z. Anorg. Allg. Chem.* **1925**, *148*, 332–344.

[26] H. Saal, M. Binnewies, M. Schrader, A. Börger, K.-D. Becker, V. A. Tikhomirov, K. Jug, *Chem. Eur. J.* **2009**, *15*, 6408–6414.

[27] D. Domide, O. Walter, S. Behrens, E. Kaifer, H.-J. Himmel, unpublished results.

[28] Y. Yang, Y. Zhao, L. Xiao, L. Zhang, *Electrochem. Commun.* **2008**, *10*, 1117–1120.

[29] DENZO-SMN, Data processing software, Nonius, **1998**; http://www.nonius.com.

[30] a) *SAINT*, Bruker AXS, **1997–2008**; b) G. M. Sheldrick, *SADABS*, Bruker AXS, **2004–2008**.

[31] a) G. M. Sheldrick, *SHELXS-97*, *Program for Crystal Structure Solution*, University of Göttingen, **1997**; http://shelx.uni-ac.gwdg.de/SHELX/index.html.

[32] a) G. Oszlányi, A. Sütö, *Acta Crystallogr., Sect. A* **2004**, *60*, 134; b) G. Oszlányi, A. Sütö, *Acta Crystallogr., Sect. A* **2005**, *61*, 147.

[33] L. Palatinus, *SUPERFLIP*, EPF Lausanne, Switzerland, **2007**; L. Palatinus, G. Chapuis, *J. Appl. Crystallogr.* **2007**, *40*, 786.

[34] G. M. Sheldrick, *SHELXL-97*, *Program for Crystal Structure Refinement*, University of Göttingen, **1997**; http://shelx.uni-ac.gwdg.de/SHELX/index.html.

[35] P. v. d. Sluis, A. L. Spek, *Acta Crystallogr., Sect. A* **1990**, *46*, 194.

[36] A. L. Spek, *PLATON*, Utrecht University, The Netherlands; A. L. Spek, *J. Appl. Crystallogr.* **2003**, *36*, 7.

[37] L. Zsolnai, G. Huttner, *XPMA*, University of Heidelberg, **1994**; http://www.uni-heidelberg.de/institute/fak12/AC/huttner/software/software.html.

[38] a) R. Ahlrichs, M. Bär, M. Häser, H. Horn, C. Kölmel, *Chem. Phys. Lett.* **1989**, *162*, 165–169; b) O. Treutler, R. Ahlrichs, *J. Chem. Phys.* **1995**, *102*, 346–354.

[39] a) A. D. Becke, *Phys. Rev. A* **1988**, *38*, 3098–3100; b) J. P. Perdew, *Phys. Rev. B* **1986**, *33*, 8822–8824.

[40] F. Weigend, R. Ahlrichs, *Phys. Chem. Chem. Phys.* **2005**, *7*, 3297–3305.

[41] K. Eichkorn, O. Treutler, H. Öhm, M. Häser, R. Ahlrichs, *Chem. Phys. Lett.* **1995**, *242*, 652–660.

[42] F. Weigend, *Phys. Chem. Chem. Phys.* **2006**, *8*, 1057–1065.

Received: January 7, 2011
Published Online: February 15, 2011

